Polymer Chemistry

RSC Publishing

PAPER

Novel polythiophene derivatives functionalized with conjugated side-chain pendants comprising triphenylamine/carbazole moieties for photovoltaic cell applications†

Cite this: *Polym. Chem.*, 2013, **4**, 506

Hsing-Ju Wang,[a] Jiann-Yu Tzeng,[b] Chen-Wei Chou,[b] Chien-Yi Huang,[b] Rong-Ho Lee*[b] and Ru-Jong Jeng*[a]

We synthesized a series of polythiophenes (PTs) featuring 2-ethylhexyl-substituted terthiophene (T) or quaterthiophene (BT) as the conjugated unit in the polymer backbone with pendant conjugated *tert*-butyl-substituted triphenylamine (*t*TPA)- or carbazole (*t*Cz)-containing moieties as side chains, namely **PT*t*TPA**, **PBT*t*TPA**, **PT*t*Cz** and **PBT*t*Cz**. Incorporating T and BT moieties into the polymer backbone and attaching *t*TPA or *t*Cz units promoted efficient conjugation within the extended conjugated frameworks of the polymers, resulting in lower band-gap energies and red-shifting of the maximal UV-Vis absorption wavelength. The higher electron-donating ability of *t*TPA resulted in broader absorption bands and lower band-gap energies of **PT*t*TPA** and **PBT*t*TPA** as compared with **PT*t*Cz** and **PBT*t*Cz**. Incorporation of the T and BT moieties into the polymer backbone enhanced the compatibility of PT and the fullerene derivative by reducing the side-chain density of PT, thus providing sufficient free volume for efficient incorporation of [6,6]phenyl-C_{61}-butyric acid methyl ester ($PC_{61}BM$) into the polymer chains. Polymer solar cells (PSCs) were fabricated by spin-coating a blend of each PT with the fullerene derivative ($PC_{61}BM$) as a composite film-type photoactive layer; **PBT*t*TPA**/$PC_{61}BM$-based PSCs showed superior photovoltaic (PV) performance to **PT*t*TPA**/$PC_{61}BM$-based PSCs in terms of conjugation and absorption band broadness. However, **PBT*t*Cz**/$PC_{61}BM$-based PSCs showed inferior PV performance to **PT*t*Cz**/$PC_{61}BM$-based PSCs. The lower HOMO level led to a higher open-circuit voltage (V_{oc}; 0.74 V) and larger photo-energy conversion efficiency (η; 2.77%) of **PT*t*Cz**/$PC_{61}BM$-based PSCs.

Received 2nd July 2012
Accepted 7th September 2012

DOI: 10.1039/c2py20477k

www.rsc.org/polymers

1 Introduction

P-type conjugated polythiophene (PT) derivatives are employed as electrically conducting polymers,[1,2] and in light-emitting diodes,[3] field-effect transistors,[4] and polymer solar cells (PSCs)[5–10] due to their excellent optical and electrical properties. Thin films fabricated from mixtures of p-type conjugated PT derivatives and n-type fullerene derivatives, such as [6,6]phenyl-C_{61}-butyric acid methyl ester ($PC_{61}BM$) or [6,6]phenyl-C_{71}-butyric acid methyl ester ($PC_{71}BM$), are currently the most successful photo-energy conversion layers for bulk heterojunction (BHJ)-type PSCs.[11] Among the p-type conjugated PTs, soluble poly(3-alkylthiophene)s, especially regioregular poly(3-hexylthiophene) (rr-P3HT), are the most widely used for applications in PSCs, but P3HT has the drawback that it only absorbs in the range from 350 to 650 nm, whereas the solar emission spectrum ranges from 350 to 1500 nm (with maximum flux at *ca.* 700 nm).[12] Furthermore, the highly ordered structure of P3HT provides satisfactory charge transport mobility, but tends to induce phase segregation in the P3HT/$PC_{61}BM$ blend.[13]

Recently, PT derivatives bearing electron-donating and -withdrawing pendant groups have been proposed for PSC applications by several groups.[14–23] PT derivatives bearing conjugated pendants possess a broad absorption band in the UV and visible regions, and so they can harvest a greater amount of solar light. Moreover, the charge mobility of the polymer is enhanced by the pendant conjugated moieties. High values of short-circuit current density (J_{sc}) and photo-energy conversion efficiency (η) have been obtained for PSCs fabricated from such conjugated polymers.[17–20] Several PTs functionalized with triphenylamine (TPA)- or carbazole-based conjugated side chains have been investigated for PSC applications.[15–17,21–26] The presence of TPA- or carbazole-based conjugated pendants is expected to enhance the conjugation of the PTs. However, the presence of these bulky pendants in PT twists the main chain

[a]*Institute of Polymer Science and Engineering, National Taiwan University, Taipei 106, Taiwan. E-mail: rujong@ntu.edu.tw; Fax: +886-2-33665237; Tel: +886-2-33665884*

[b]*Department of Chemical Engineering, National Chung Hsing University, Taichung 402, Taiwan. E-mail: rhl@dragon.nchu.edu.tw; Fax: +886-4-22854734; Tel: +886-4-22854308*

† Electronic supplementary information (ESI) available. See DOI: 10.1039/c2py20477k

out of planar π-conjugation and decreases the effective conjugation length of the polymer backbone.[16,21–26] As a result, the band-gap energies of these PTs are increased, and are unfavorable for harvesting solar light.[16] Moreover, due to the steric hindrance of the bulky conjugated moiety, the conjugated pendant-containing monomer shows low reactivity and poor solubility, resulting in a lower molecular weight of the synthesized PTs.[26,27] The steric effect of the bulky conjugated pendants also results in poor compatibility between the polymer and $PC_{61}BM$,[21,26] reducing the photovoltaic (PV) performance of the corresponding PSCs. Therefore, we considered that the key points for obtaining superior PTs for PSC applications are to improve the absorption intensity and conjugation length of PT, to further compatibilize the blend components by reducing the steric hindrance due to the pendant moieties, and to increase the solubility of the monomer.[28,29] Here, we synthesized a series of PTs featuring two different conjugated units, *i.e.*, 2-ethylhexyl-substituted terthiophene (T) and quaterthiophene (BT), in the polymer backbone and with pendant conjugated triphenylamine- or carbazole-containing moieties substituted with *tert*-butyl groups (*t*TPA and *t*Cz, respectively) as side chains, namely **PT*t*TPA**, **PBT*t*TPA**, **PT*t*Cz** and **PBT*t*Cz**. PTs in this study are illustrated in Fig. 1. The *t*TPA and *t*Cz groups have excellent electron-donating ability and serve to increase the conjugation length and charge mobility of the polymer. The presence of *tert*-butyl groups is favorable for the conjugated polymer to be more soluble. A homogenous amorphous polymer film would be obtained for the *tert*-butyl groups containing a conjugated polymer based photoactive layer.[30] We expected that the introduction of T and BT units into the polymer backbone of PTs would reduce the steric crowding between adjacent bulky pendant moieties and thus would enhance the coplanarity of the polymer backbone and bulky pendants. These structural features should improve intramolecular conjugation within the conjugated frameworks of the polymers, lower the band-gap energies and broaden the absorption range of PTs. Further, the inclusion of 2-ethylhexyl substituents on the conjugated T and BT units should improve the solubility of the PTs, and increased solubility of PTs should improve the quality of thin films prepared from PT/$PC_{61}BM$ blends. We further expected that the photophysical and electrochemical behaviors of these polymers would be easily tunable by controlling the extent of incorporation of *t*TPA- and *t*Cz-containing conjugated pendant moieties.

To validate these ideas, we synthesized **PT*t*TPA**, **PBT*t*TPA**, **PT*t*Cz** and **PBT*t*Cz** and used UV-Vis absorption spectroscopy and cyclic voltammetry (CV) to study the effects of the T and BT conjugation segments on the photophysical and electrochemical properties of the polymers. We also employed atomic force microscopy (AFM) and transmission electron microscopy (TEM) to study the morphology of thin films prepared from *t*TPA- and *t*Cz-functionalized PT/$PC_{61}BM$ blends. We then fabricated PSCs having a conventional indium tin oxide (ITO)-coated glass/hole-transporting medium (HTM)/photoactive layer/LiF (0.5 nm)/Al (100 nm) structure, by spin-coating a blend

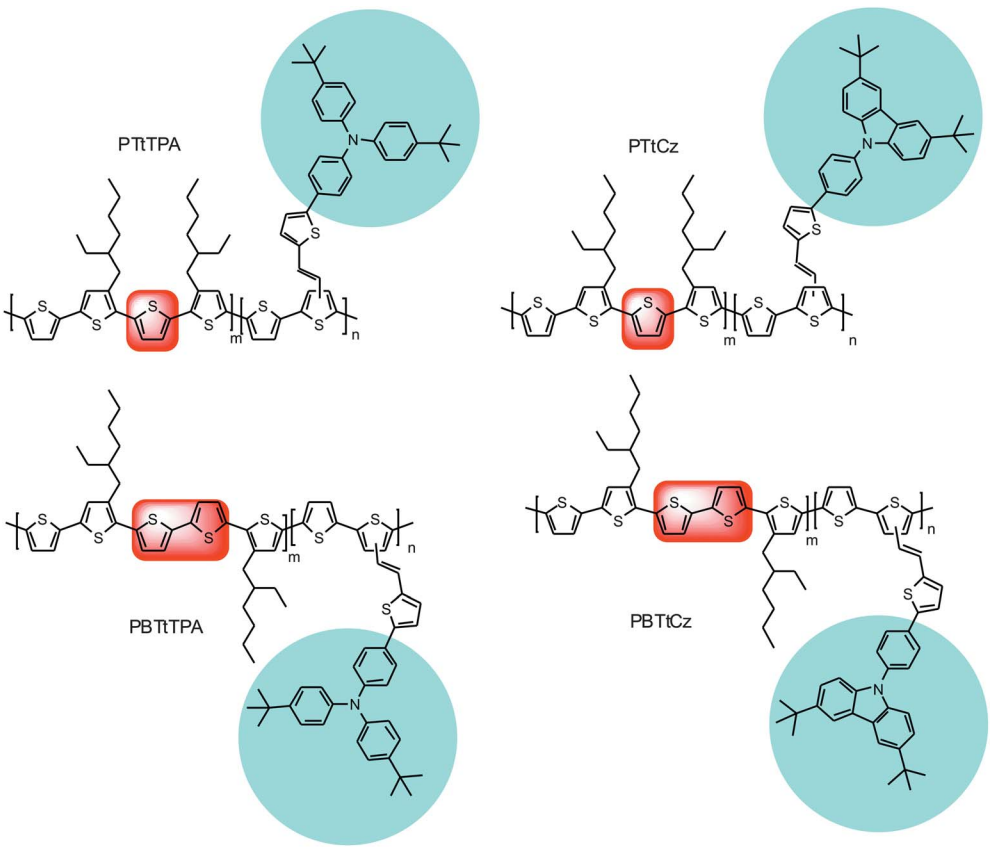

Fig. 1 Illustrations of **PT*t*TPA**, **PBT*t*TPA**, **PT*t*Cz** and **PBT*t*Cz**.

of each PT with $PC_{61}BM$ (w/w = 1 : 1) to form a composite film-type photoactive layer on an HTM layer deposited on ITO-coated glass. The PV performance of these PSCs was evaluated, and, based on the results, we discuss the influence of the molecular-structural features of our PTs on PSC performance.

2 Experimental details

2.1 Chemicals

Bis(4-*tert*-butylphenyl)amine, 9*H*-carbazole, 2-chloro-2-methylpropane, *n*-butyllithium (2.5 M in hexane), CH_3MgBr (3 M in THF) and other reagents and chemicals were purchased from Aldrich, Alfa and TCI Chemical Co., and used as received. Dichloromethane (DCM), tetrahydrofuran (THF), dimethylformamide (DMF), nitromethane, toluene, and *o*-dichlorobenzene (*o*-DCB) were freshly distilled over appropriate drying agents prior to use as solvents, and were purged with nitrogen. The *tert*-butyl-substituted triphenylamine- and carbazole-containing moieties (*t*TPA and *t*Cz) and 2-ethylhexyl-substituted terthiophene and quaterthiophene moieties (T and BT) were synthesized as shown in Schemes 1 and 2, respectively. Syntheses of **PT*t*TPA**, **PBT*t*TPA**, **PT*t*Cz**, and **PBT*t*Cz** are illustrated in Scheme 3. Diethyl(2,5-dibromothiophen-3-yl) methylphosphonate (**8**), 2-bromo-3-(2-ethylhexyl)thiophene,[31]

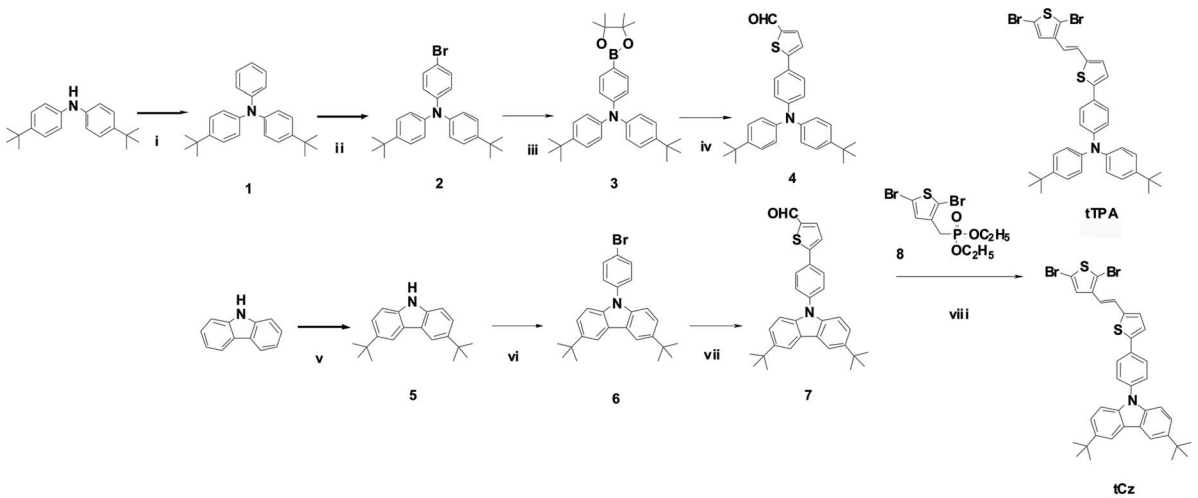

Scheme 1 Synthesis of the aromatic amine pendants (*t*TPA and *t*Cz) (i) CH_3MgBr, reflux in THF for 3 h, afterward PPh_3, bromobenzene reflux in toluene 8 h; (ii) NBS, 0 °C, DCM, 30 min; (iii) *n*-BuLi 1 h, afterward trimethylborate 2 h, −78 °C → 0 °C, then pinacol, toluene, reflux, 8 h; (iv) 5-bromo-2-thiophenecarboxaldehyde, K_2CO_3 (2 M, aq.), $Pd(PPh_3)_4$, toluene, 24 h, reflux; (v) $ZnCl_2$, 2-chloro-2-methylpropane, nitromethane, 25 °C, 5 h; (vi) 1,4-dibromobenzene, K_2CO_3, Cu, 18-crown-6-ether, *o*-DCB, 180 °C, 8 h; (vii) thiophene-2-carboxaldehyde, KOAc, $Pd(OAc)_2$, DMAc, 180 °C, 20 h, (viii) CH_3ONa, DMF, 0 °C, 2 h.

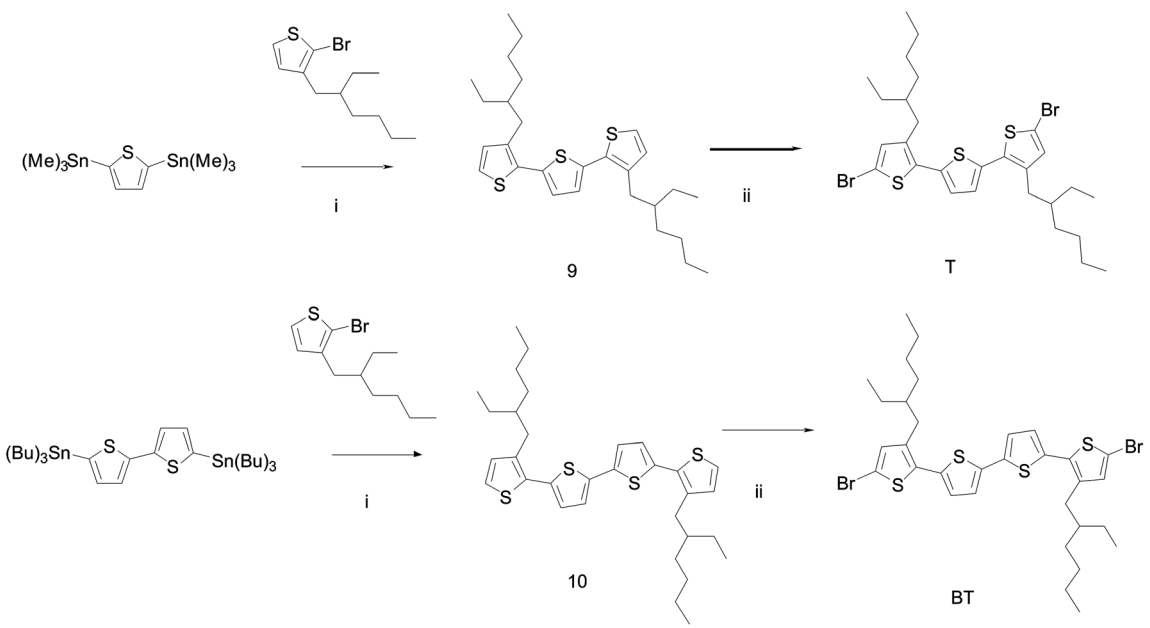

Scheme 2 Synthesis of π-conjugated units (T and BT) (i) $Pd(PPh_3)_4$, toluene, 24 h, reflux; (ii) NBS, 0 °C, DMF.

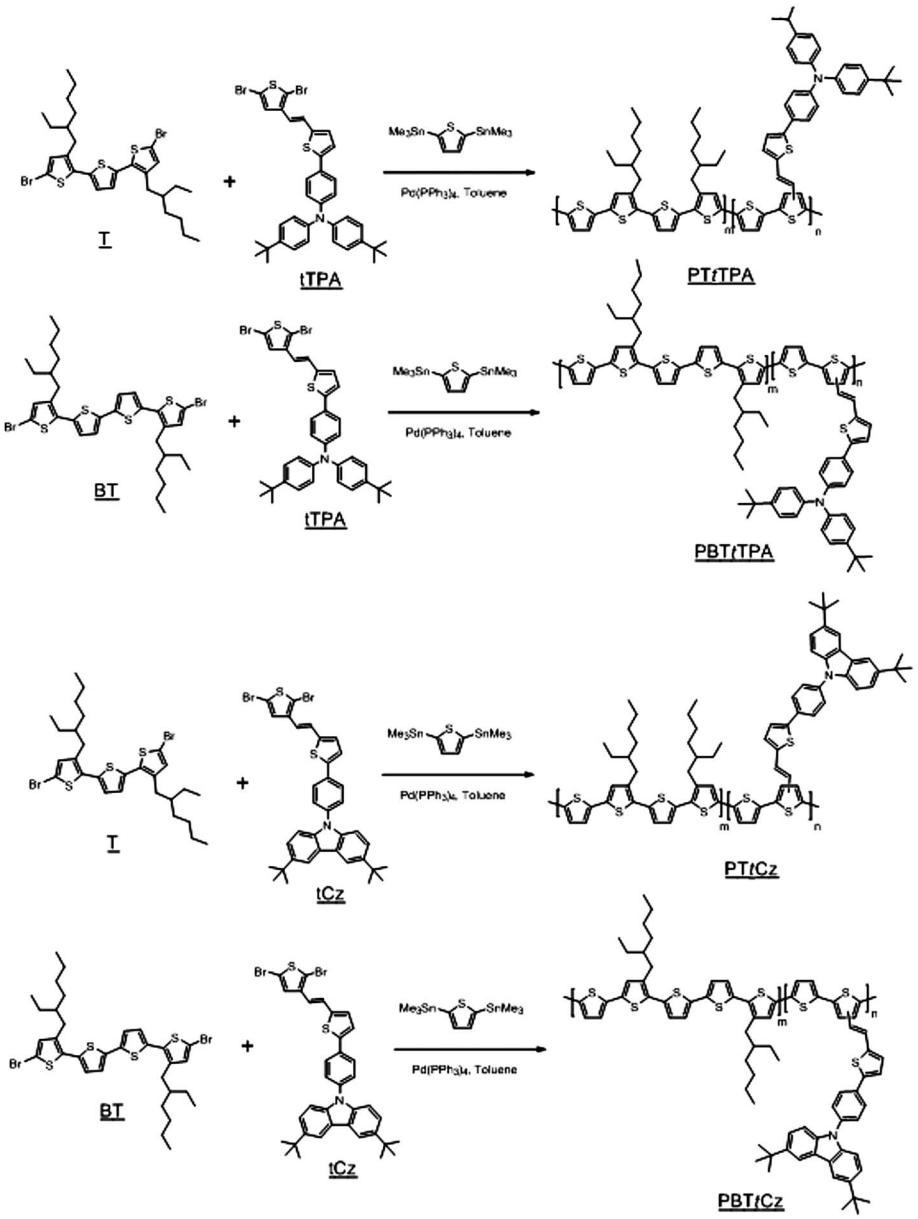

Scheme 3 Polymerization of PTs.

2,5-bis(trimethylstannyl)thiophene,[21,32] and 5,5′-bis(tributylstannyl)-2,2′-bithiophene[33] were synthesized according to the literature.

2.2 Synthesis

(4,4′-Di-*tert*-butyl)triphenylamine (1). A solution of bis(4-*tert*-butylphenyl)amine (2.81 g, 10 mmol) in dry THF (60 mL) was stirred at 0 °C under N_2 for 10 min and then CH_3MgBr (4.16 mL, 12.5 mmol) was added dropwise. The solution was heated under reflux with stirring for 3 h. After cooling to room temperature, it was evaporated to dryness, and the residue was dissolved in dry toluene (60 mL) under N_2. Triphenylphosphine (0.47 g, 1 mmol) and bromobenzene (1.58 mL, 15 mmol) were added, and the mixture was refluxed for 8 h. Methanol was added to quench the reaction. The mixture was partitioned between ethyl acetate (EA) and water, and the organic phase was dried ($MgSO_4$), filtered, and evaporated to dryness. The residue was purified chromatographically (SiO_2; hexane) to provide a white solid (2.6 g, 73%). ^{1}H-NMR (δ/ppm, 400 MHz, $CDCl_3$): 1.31 (s, 18H), 6.90–7.10 (m, 7H), 7.15–7.30 (m, 6H). Anal. calcd for $C_{26}H_{31}N$: C, 87.39; H, 8.68; N, 3.92. Found: C, 87.41; H, 8.64; N, 3.89%.

(4,4′-Di-*tert*-butyl-4″-bromo)triphenylamine (2). A solution of **1** (3.58 g, 10 mmol) in 20 mL DCM was stirred in an ice-water bath for 15 minutes. *N*-Bromosuccinimide (1.77 g, 10 mmol) in 20 mL DCM was added dropwise to the solution over 15 min at 0 °C. The mixture was warmed to room temperature and stirred for 2 h, then Na_2SO_3 aqueous solution was added to quench the reaction. The mixture was partitioned between DCM and water, and the organic phase was dried ($MgSO_4$), filtered, and evaporated to dryness. The residue was recrystallized (MeOH–DCM)

to provide a white solid (3.06 g, yield = 70%). ^{1}H-NMR (δ/ppm, 400 MHz, $CDCl_3$): 1.35 (s, 18H), 6.91–7.10 (m, 6H), 7.23–7.32. (m, 6H). Anal. calcd for $C_{26}H_{30}NBr$: C, 71.72; H, 8.89; N, 3.22. Found: C, 71.70; H, 8.93; N, 3.27%.

(4,4′-Di-*tert*-butyl-4″-(4,4,5,5-tetramethyl-1,3,2-dioxaborolan-2-yl))triphenylamine (3). A solution of **2** (4.37 g, 10 mmol) in dry THF (35 mL) was stirred at −78 °C under a N_2 atmosphere and then *n*-BuLi (2.5 M in hexane, 4 mL, 10 mmol) was added dropwise. The mixture was maintained at −78 °C with stirring for a further 3 h, during which trimethyl borate (1.47 mL, 13 mmol) was added dropwise. The mixture was warmed to room temperature and stirred for 8 h, then HCl (1 N) was added to quench the reaction. The resulting mixture was partitioned between EA and water, and the organic phase was dried ($MgSO_4$), filtered, and evaporated to dryness. The residue was then dissolved in toluene (100 mL). Pinacol (1.78 g, 15 mmol) was added to this solution, and the mixture was stirred under reflux for 8 h. After cooling to room temperature, it was partitioned between EA and water, and the organic phase was dried ($MgSO_4$), filtered, and evaporated to dryness. The residue was purified chromatographically (SiO_2; EA–hexane = 1 : 20) to provide a yellowish oil (2.86 g, yield = 67%). ^{1}H-NMR (δ/ppm, 400 MHz, $CDCl_3$): 1.20–1.40 (m, 30H), 6.97–7.05 (d, 6H), 7.22–7.26 (d, 4H), 7.60–7.62 (d, 2H). Anal. calcd for $C_{32}H_{42}NBO_2$: C, 79.53; H, 8.70; N, 29.0; O, 6.63. Found: C, 79.43; H, 8.75; N, 29.3; O, 6.23%.

5-(4-(Bis(4-*tert*-butylphenyl)amino)phenyl)thiophene-2-carbaldehyde (4). A mixture of **3** (4.82 g, 10 mmol) and 5-bromo-2-thiophene-carboxaldehyde (1.91 g, 10 mmol) in dry toluene (80 mL) was flushed with N_2 for 30 min and then K_2CO_3 aqueous solution (2 M, 18 mL) and $Pd(PPh_3)_4$ (0.23 g, 0.2 mmol) were added. The reaction mixture was stirred under reflux for 24 h. After cooling to room temperature, the mixture was partitioned between EA and water, and the organic phase was dried ($MgSO_4$), filtered, and evaporated to dryness. The residue was purified chromatographically (EA–hexane = 1 : 10) to provide a yellow solid (3.37 g, yield = 72%). ^{1}H-NMR (δ/ppm, 400 MHz, d-DMSO): 1.25–1.32 (s, 18H), 7.1 (d, 6H), 7.20–7.28 (m, 5H), 7.46 (d, 2H), 7.65 (d, 1H), 9.84 (s, 1H). Anal. calcd for $C_{31}H_{33}NOS$: C, 79.66; H, 7.07; N, 3.00; O, 3.43. Found: C, 79.78; H, 7.01; N, 3.10; O, 3.40%.

3,6-Di-*tert*-butyl-9*H*-carbazole (5). A mixture of 9*H*-carbazole (1.67 g, 10 mmol) and $ZnCl_2$ (4.08 g, 30 mmol) in nitromethane (17 mL) was stirred for several minutes, then 2-chloro-2-methylpropane (3.279 g, 30 mmol) in nitromethane (3 mL) was added dropwise. The reaction solution was stirred under N_2 at room temperature for 5 h, then partitioned between EA and water, and the organic phase was dried ($MgSO_4$), filtered, and evaporated to dryness. The residue was recrystallized (MeOH–DCM) to provide a yellowish solid (2.1 g, yield = 75%). ^{1}H-NMR (δ/ppm, 400 MHz, $CDCl_3$): 1.30–1.31 (s, 18H), 7.32 (d, 2H), 7.42 (d, 2H), 7.58 (br, 1H), 8.06 (s, 2H). Anal. calcd for $C_{18}H_{25}N$: C, 84.71; H, 9.80; N, 5.49. Found: C, 84.74; H, 9.75; N, 5.52%.

3,6-Di-*tert*-butyl-9-(4-bromophenyl)carbazole (6). A mixture of **5** (2.79 g, 10 mmol), 1,4-dibromobenzene (7.89 g, 33.5 mmol), K_2CO_3 (5.52 g, 40 mmol), copper (0.425 g, 6.7 mmol), and 18-crown-6-ether (8.7 g, 3.3 mmol) in dry *o*-dichlorobenzene (50 mL) was stirred at 180 °C for 8 h, then partitioned between EA and water. The organic phase was dried ($MgSO_4$), filtered, and evaporated to dryness. The residue was purified chromatographically (hexane) to provide a white solid (3.08 g, yield = 71%). ^{1}H-NMR (δ/ppm, 400 MHz, $CDCl_3$): 1.30–1.31 (s, 18H), 7.29 (d, 2H), 7.41–7.45 (m, 4H), 7.68 (d, 2H), 8.16 (d, 2H). Anal. calcd for $C_{26}H_{28}NBr$ 433: C, 72.06; H, 6.47; N, 3.23. Found: C, 72.18; H, 6.43; N, 3.26%.

5-(4-(3,6-Di-*tert*-9-carbazolyl)phenyl)thiophene-2-carbaldehyde (7). A mixture of **6** (4.34 g, 10 mmol), thiophene-2-carbaldehyde (1.81 mL, 20 mmol), KOAc (1.96 g, 20 mmol), and $Pd(OAc)_2$ (0.2 g, 1 mmol) in dry DMAc (70 mL) was stirred at 180 °C for 20 h, then DMAc was removed with the aid of a vacuum system. The crude product was partitioned between EA and water, and the organic phase was dried ($MgSO_4$), filtered, and evaporated to dryness. The residue was purified chromatographically (EA–hexane = 1 : 10) to provide a yellow solid (2.93 g, yield = 63%). ^{1}H-NMR (δ/ppm, 400 MHz, $CDCl_3$): 1.41 (s, 18H), 7.40 (d, 1H), 7.41–7.43 (m, 4H), 7.61 (d, 2H), 7.78 (d, 1H), 7.82 (d, 2H), 8.16 (s, 2H), 9.91 (s, 1H). Anal. calcd for $C_{31}H_{31}NOS$: C, 80.00; H, 6.67; N, 3.01; O, 3.44. Found: C, 80.22; H, 6.57; N, 3.11; O, 3.40%.

(*E*)-4-(5-(2-(2,5-Dibromothiophen-3-yl)vinyl)thiophen-2-yl)-*N*,*N*-((4,4′-di-*tert*-butyl)diphenyl)aniline (*t*TPA). A solution of **8** (4.31 g, 11 mmol) in DMF (20 mL) was stirred in an ice-water bath for several minutes and then CH_3ONa (1.62 g, 30 mmol) in DMF (50 mL) was added dropwise. After 20 min, the reaction solution turned brown. Then, a solution of **4** (4.67 g, 10 mmol) in DMF (20 mL) was added dropwise. The mixture was warmed to room temperature and stirred for 2 h, then MeOH was added to quench the reaction. The crude product was partitioned between EA and water, and the organic phase was dried ($MgSO_4$), filtered, and evaporated to dryness. The residue was purified chromatographically (EA–hexane = 1 : 10) to provide a yellow solid (5.72 g, yield = 81%). ^{1}H NMR (δ/ppm, 400 MHz, $CDCl_3$) 1.36 (s, 18H), 6.76 (d, 1H), 6.94–7.05 (d, 8H), 7.09 (d, 1H), 7.14 (d, 1H), 7.26 (d, 4H), 7.42 (s, 2H). Anal. calcd for $C_{36}H_{35}Br_2NS_2$: C, 61.28; H, 4.96; N, 1.99; S, 9.08. Found: C, 61.39; H, 4.98; N, 2.01; S, 8.97%.

3,6-Di-*tert*-butyl-9-(4-((*E*)-4-(5-(2-(2,5-dibromothiophen-3-yl)vinyl)thiophen-2-yl))phenyl)carbazole (*t*Cz). A solution of **8** (4.31 g, 11 mmol) in DMF (20 mL) was stirred in an ice-water bath for several minutes and then CH_3ONa (1.62 g, 30 mmol) in DMF (50 mL) was added dropwise. After 20 min, the reaction solution turned brown. Then, a solution of **7** (4.65 g, 10 mmol) in DMF (20 mL) was further added dropwise. The mixture was warmed to room temperature and stirred for 2 h, and MeOH was added to quench the reaction. The crude product was partitioned between EA and water, and the organic phase was dried ($MgSO_4$), filtered, and evaporated to dryness. The residue was purified chromatographically (EA–hexane = 1 : 10) to provide a yellow solid (5.56 g, yield = 79%). ^{1}H NMR (δ/ppm, 400 MHz, $CDCl_3$): 1.45 (s, 18H), 6.80–7.03 (q, 2H), 7.08 (d, 1H),7.17 (s, 1H), 7.29 (d, 1H), 7.37 (d, 2H), 7.44 (d, 2H), 7.57 (d, 2H), 7.80 (d, 2H), 8.17 (s, 2H). Anal. calcd for $C_{36}H_{33}NS_2Br_2$: C, 61.45; H, 4.69; N, 1.99; S 9.10. Found: C, 61.55; H, 4.65; N, 2.01; S, 8.95%.

3,3′′-Diethylhexyl-2,2′;5′,2′′-terthiophene (9). A mixture of 2-bromo-3-(2-ethylhexyl)thiophene (7.14 g, 25 mmol), 2,5-bis-(trimethylstannyl)thiophene (4.09 g, 10 mmol), and $Pd(PPh_3)_4$ (0.3 g, 0.25 mmol) in dry toluene (100 mL) was stirred under reflux for 24 h. After it had cooled to room temperature, the mixture was partitioned between EA and water, and the organic phase was dried ($MgSO_4$), filtered, and evaporated to dryness. The residue was purified chromatographically (hexane) to provide a yellowish liquid (3.26 g, 69%). ^{1}H NMR (δ/ppm, 400 MHz, $CDCl_3$): 0.75–0.84 (m, 12H), 1.23–1.31 (m, 16H), 1.63 (s, 2H), 2.68–2.71 (d, 4H), 6.85 (d, 2H), 7.02 (s, 2H), 7.18 (d, 2H). Anal. calcd for $C_{28}H_{40}S_3$: C, 71.19; H, 8.47; S, 20.34. Found: C, 71.27; H, 8.44; S, 20.15%.

5,5′′-Dibromo-3,3′′-diethylhexyl-2,2′;5′,2′′-terthiophene (T). A solution of **9** (4.72 g, 10 mmol) in DMF (25 mL) was stirred in an ice water bath for 15 minutes, then *N*-bromosuccinimide (3.55 g, 20 mmol) in DMF (40 mL) was added dropwise over 15 min at 0 °C. The mixture was warmed to room temperature and stirred for 2 h, then Na_2SO_3 aqueous solution was added to quench the reaction. The mixture was partitioned between EA–water, and the organic phase was dried ($MgSO_4$), filtered, and evaporated to dryness. The residue was purified chromatographically (hexane) to provide a yellow liquid (5.36 g, 85%). ^{1}H NMR (δ/ppm, 400 MHz, $CDCl_3$): 0.76–0.87 (m, 12H), 1.26–1.31 (m, 16H), 1.62 (s, 2H), 2.70 (d, 4H), 6.86 (d, 2H), 7.01 (s, 2H), 7.08 (d, 2H). Anal. calcd for $C_{30}H_{40}Br_2S_3$: C, 55.05; H, 6.12; S, 14.68. Found: C, 55.14; H, 6.10; S, 14.65%.

3,3′′′-Diethylhexyl-2,2′;5′,2′′;5′′,2′′′-quaterthiophene (10). A mixture of 2-bromo-3-(2-ethylhexyl)thiophene (7.14 g, 25 mmol), 5,5′-bis(tributylstannyl)-2,2′-bithiophene (3.24 g, 10 mmol), and $Pd(PPh_3)_4$ (0.3 g, 0.25 mmol) in dry toluene (100 mL) was stirred under reflux for 24 h. After it had cooled to room temperature, the mixture was partitioned between EA and water, and the organic phase was dried ($MgSO_4$), filtered, and evaporated to dryness. The residue was purified chromatographically (hexane) to provide a yellowish liquid (3.66 g, 66%). ^{1}H NMR (δ/ppm, 400 MHz, $CDCl_3$): 0.81–0.84 (m, 12H), 1.23–1.42 (m, 16H), 1.62–1.65 (s, 2H), 2.65 (d, 4H), 6.88 (d, 2H), 6.99 (d, 2H), 7.15 (d, 2H), 7.17 (d, 2H). Anal. calcd for $C_{32}H_{42}S_4$: C, 69.31; H, 7.58; S, 23.10. Found: C, 69.42; H, 7.51; S, 23.05%.

5,5′′′-Dibromo-3,3′′′-diethylhexyl-2,2′;5′,2′′;5′′,2′′′-quaterthiophene (BT). A solution of **10** (5.54 g, 10 mmol) in DMF (25 mL) was stirred in an ice water bath for 15 minutes, then *N*-bromosuccinimide (3.55 g, 20 mmol) in DMF (40 mL) was added dropwise over 15 min at 0 °C. The mixture was warmed to room temperature and stirred for 6 h, and Na_2SO_3 aqueous solution was added to quench the reaction. The mixture was partitioned between EA and water, and the organic phase was dried ($MgSO_4$), filtered, and evaporated to dryness. The residue was purified chromatographically (hexane) to provide a yellow liquid (5.40 g, 76%). ^{1}H NMR (δ/ppm, 400 MHz, $CDCl_3$): 0.81–0.84 (br, 12H), 1.06–1.38 (br, 16H), 1.60 (s, 2H), 2.6 (d, 4H), 6.82 (s, 2H), 6.93 (d, 2H), 7.07 (d, 2H). Anal. calcd for $C_{32}H_{40}Br_2S_4$: C, 54.08; H, 5.63; S, 18.03. Found: C, 54.12; H, 5.65; S, 17.78%.

PT*t*TPA. A mixture of 2,5-bis(trimethylstannyl)thiophene (0.62 g, 1.5 mmol), T (0.47 g, 0.75 mmol), and *t*TPA (0.53 g, 0.75 mmol), and $Pd(PPh_3)_4$ (0.018 g, 0.015 mmol) in dry toluene (25 mL) was stirred at reflux temperature for 48 h, then poured into methanol (100 mL). The precipitated material was filtered into a Soxhlet thimble and extracted with methanol, hexane, acetone, and chloroform. The polymer was recovered from the chloroform fraction by rotary evaporation. Drying under vacuum for 24 h provided a black solid (0.74 g, 83%). ^{1}H-NMR (δ/ppm, 400 MHz, d-DCM): 0.60–1.0 (br, 30H), 1.00–1.42 (br, 18H), 2.65–2.80 (br, 4H), 6.60–7.40 (br, 25H). Anal. calcd for $(C_{32}H_{40}S_4)(C_{40}H_{37}NS_3)$: C, 73.28; H, 6.53; N, 1.19; S, 19.0. Found: C, 73.35; H, 6.56; N, 1.21; S, 18.4%.

PBT*t*TPA. Using the same procedure as that described for the synthesis of **PT*t*TPA**, the reaction of 2,5-bis(trimethylstannyl) thiophene (0.62 g, 1.5 mmol), BT (0.54 g, 0.75 mmol), and *t*TPA (0.53 g, 0.75 mmol) provided a black solid (0.72 g, 75%). ^{1}H-NMR (δ/ppm, 400 MHz, d-DCM): 0.80–1.05 (br, 35H), 1.15–1.41 (br, 25H), 2.65–2.74 (br, 5H), 6.50–7.60 (br, 30H). Anal. calcd for $(C_{36}H_{42}S_5)_{1.38}(C_{40}H_{37}NS_3)$: C, 71.65; H, 6.32; N, 0.93; S, 21.09. Found: C, 71.82; H, 6.37; N, 0.82; S, 20.19%.

PT*t*Cz. Using the same procedure as that described for the synthesis of **PT*t*TPA**, the reaction of 2,5-bis(trimethylstannyl) thiophene (0.62 g, 1.5 mmol), T (0.47 g, 0.75 mmol), and *t*Cz (0.53 g, 0.75 mmol) provided a deep-red solid (0.68 g, 76%). ^{1}H-NMR (δ/ppm, 400 MHz, d-DCM): 0.91 (br, 38H), 1.10–1.45 (br, 30H), 2.61–2.78 (br, 7H), 6.40–7.80 (br, 25H), 7.90–8.21 (br, 2H). Anal. calcd for $(C_{32}H_{40}S_4)_{1.67}(C_{40}H_{35}NS_3)$: C, 72.49; H, 6.57; N, 0.93; S, 20.00. Found: C, 72.47; H, 6.54; N, 0.97; S, 19.98%.

PBT*t*Cz. Using the same procedure as that described for the synthesis of **PT*t*TPA**, the reaction of 2,5-bis(trimethylstannyl) thiophene (0.62 g, 1.5 mmol), BT (0.54 g, 0.75 mmol), and *t*Cz (0.53 g, 0.75 mmol) provided a dark-red solid (0.73 g, 76%). ^{1}H-NMR (δ/ppm, 400 MHz, d-DCM): 0.91 (br, 35H), 1.10–1.45 (br, 26H), 2.61–2.78 (br, 6H), 6.20–7.77 (br, 27H), 7.90–8.21 (br, 2H). Anal. calcd for $(C_{36}H_{42}S_5)_{1.46}(C_{40}H_{35}NS_3)$: C, 71.63; H, 6.20; N, 0.90; S, 21.25. Found: C, 71.61; H, 6.15; N, 0.92; S, 21.31%.

2.2 Characterization of copolymers

^{1}H NMR (400 MHz) spectra were recorded using a Varian Unity Inova spectrometer. The average molecular weights of the polymers were measured by means of GPC on a Waters chromatography system (717 plus Autosampler) equipped with two Waters Styragel linear columns. Polystyrene standards were used, with THF as the eluent. The glass transition temperature (T_g) and thermal decomposition temperature (T_d; temperature at which weight loss reaches 5%) of the copolymers were determined by means of differential scanning calorimetry (TA Instruments, DSC-2010) and thermogravimetric analysis (TA Instruments, TGA-2050), respectively. Both analyses were performed under a N_2 atmosphere at a scanning (both heating and cooling) rate of 10 °C min^{-1}. The temperatures at the intercepts of the curves in the thermogram (endothermic, exothermic, or weight loss) with the leading baseline were taken as estimates of T_g and T_d. Absorption spectra were measured using a Hitachi U3010 UV-Vis spectrometer. Fluorescence spectra were measured using a Varian Cary Eclipse luminescence spectrometer. Dilute *o*-DCB solutions of the PTs were filtered

through a 0.45 μm filter to remove insoluble materials before spectral measurements. Redox potentials of the polymers were determined with a CHI 611D electrochemical analyzer (scanning rate: 50 mV s^{-1}) equipped with Pt electrodes and an Ag/Ag^+ (0.10 M $AgNO_3$ in MeCN) reference electrode in an anhydrous, N_2-saturated solution of 0.1 M Bu_4NClO_4 in MeCN. Bu_4NClO_4 (98%, TCI) was recrystallized three times from MeOH and water (1 : 1) and then dried at 100 °C under reduced pressure. A Pt plate coated with a thin polymer film was used as the working electrode; a Pt wire and an Ag/Ag^+ electrode were used as the counter and reference electrodes, respectively. The electrochemical potential was calibrated against ferrocene/ferrocenium. The morphology of films prepared from PT/$PC_{61}BM$ blends was studied using an atomic force microscope (AFM, Seiko SII SPA400) operated in the tapping mode and a transmission electron microscope (TEM, JEOL JEM-1400).

2.3 Fabrication and characterization of PSCs

The PSCs fabricated in this study had an indium tin oxide (ITO)-coated glass/hole-transporting material (HTM)/photoactive layer/LiF (0.5 nm)/Al (100 nm) structure, in which the photoactive layer consisted of an interpenetrating network of PT and the fullerene derivative $PC_{61}BM$. ITO-coated glass (sheet resistance: 20 Ω sq^{-1}) was purchased from Applied Film Corp. $PC_{61}BM$ was purchased from American Dye Source and used as received. The PSCs were fabricated as follows: glass substrates with patterned ITO electrodes were washed well and then cleaned by means of O_2 plasma treatment. A thin film of the HTM, poly(3,4-ethylenedioxythiophene) doped with poly(styrene sulfonate) (PEDOT:PSS, AI4083, Heraeus Clevios GmbH), was deposited on the ITO layer by using the spin-casting method. The sample was dried at 150 °C for 30 min in a glove box. A mixture solution of PT and $PC_{61}BM$ (34 mg mL^{-1} in *o*-DCB) was stirred overnight, then filtered through a 0.2 μm poly(tetrafluoroethylene) (PTFE) filter and spin-coated (1500 rpm, 30 s) onto the HTM layer to prepare the PT/$PC_{61}BM$ composite film-based photo-active layer. The sample was dried at 110 °C for 10 min in a glove box. In a high-vacuum chamber, the LiF/Al-based cathode was thermally deposited onto the PT/$PC_{61}BM$ composite layer. The active area of the PSC was 0.04 cm^2. After electrode deposition, the PSC was encapsulated. The cathode deposition rate was determined using a quartz thickness monitor (STM-100/MF, Sycon). The thickness of thin films was determined using a surface texture analysis system (3030ST, Dektak). The PV properties of the PSCs were measured using a programmable electrometer equipped with current and voltage sources (Keithley 2400) under illumination with solar-simulating light (100 mW cm^{-2}) from an AM1.5 solar simulator (NewPort Oriel 96000).

3 Results and discussion

3.1 Characterization of PTs

The repeat unit ratio (*m*/*n*; see Fig. 1) of the PTs **PT*t*TPA**, **PBT*t*TPA**, **PT*t*Cz**, and **PBT*t*Cz** was modulated by controlling the feed ratio of the conjugation unit T or BT, and the actual values of *m*/*n* were determined from the relative integral areas of the peaks at 6.20–8.21 ppm (due to protons of the vinylene, phenyl, carbazolyl, and thiophene groups) and 0.60–2.87 (due to protons of the *tert*-butyl and 2-ethylhexyl groups) in the ^1H NMR spectra of the copolymers. The values of *m*/*n* of **PT*t*TPA**, **PBT*t*TPA**, **PT*t*Cz**, and **PBT*t*Cz** were approximately 1 : 1, 1.38 : 1, 1.67 : 1, and 1.46 : 1, respectively. One reason for the higher *m*/*n* ratios of **PT*t*Cz** and **PBT*t*Cz**, compared with **PT*t*TPA** and **PBT*t*TPA**, might be the fact that the polymerization involves an oxidative addition step, and the addition is more likely to occur at a more highly conjugated unit.[14] *t*TPA has both a higher electron-donating ability and better oxidative addition capacity than *t*Cz. On the other hand, poor solubility of the *t*Cz-containing segment would inhibit the propagation of the polymer chains, and a higher content of *t*Cz-containing segments would lead to precipitation at the initial stages of polymerization, resulting in **PT*t*Cz** and **PBT*t*Cz** with a higher *m*/*n* ratio.[26] Using GPC with THF as the eluent and polystyrene internal standards, we determined the number-average molecular weight (M_n) and weight-average molecular weight (M_w) of the conjugated PTs. As summarized in Table 1, the values of M_n and M_w of the conjugated polymers are in the ranges of 8.2–18.6 (kg mol^{-1}) and 28.4–73.1 (kg mol^{-1}), respectively.

All of the conjugated copolymers were soluble in common organic solvents, including chloroform, THF, and *o*-DCB. In general, conjugated polymers have poor solubility due to strong π–π interaction between planar polymer backbones. A frequently employed strategy to improve the solubility of such polymers is substitution with linear alkyl chains. However, in the present polymers, the branched 2-ethylhexyl side-chains were more effective in improving the solubility. Another potential issue is early termination of propagation of polymer chains due to the poor solubility of the polymer in the reaction solution, resulting in precipitation of the polymer. Indeed, we were unable to synthesize simple carbazole-substituted PT, but

Table 1 Molecular weight, optical properties, electrochemical onset potentials, and electronic energy levels of the PTs

PTs	M_n (kg mol^{-1})	M_w (kg mol^{-1})	$\lambda_{max}^{abs\ a}$ (nm)	$\lambda_{max}^{abs\ b}$ (nm)	$\lambda_{onset}^{abs\ c}$ (nm)	$E_g^{opt d}$ (eV)	E_{on}^{ox} (V)	HOMO (eV)	LUMO (eV)
PT*t*TPA	18.6	73.1	448	559	752	1.65	0.42	−5.13	−3.48
PBT*t*TPA	8.2	28.4	453	564	785	1.58	0.40	−5.11	−3.53
PT*t*Cz	11.2	43.3	420	524	689	1.80	0.45	−5.16	−3.36
PBT*t*Cz	12.0	47.9	471	529	701	1.77	0.43	−5.14	−3.37

[a] The maximal absorption wavelength of the polymer in solution. [b] The maximal absorption wavelength of the polymer as thin film. [c] The onset of UV-vis absorption of the polymer as thin film. [d] Calculated E_g from the onset absorption (λ) of the polymer thin film: $E_g = 1240/\lambda_{onset}^{abs}$.

tert-butyl substitution of the carbazole allowed successful synthesis of **PT*t*Cz** and **PBT*t*Cz** through the Stille coupling reaction. **PT*t*Cz** and **PBT*t*Cz** with *t*Cz pendants exhibited good solubility in saturated hydrocarbons (hexane and pentane). In addition, higher values of polydispersity index (PDI) were observed for these conjugated side-chain containing PTs than for main-chain type PTs, presumably due to the multiple thiophene rings in the co-monomers T and BT. In other words, the larger molecular sizes of T and BT, as compared to 2,5-dibromothiophene, resulted in higher PDI values of PTs.

The operational stability of PSCs is directly related to the thermal stability of the component conjugated polymer. Thus, high values of T_g and T_d are desirable. We measured the T_g and T_d of our conjugated copolymers by means of thermal analyses using DSC and TGA, as shown in Fig. S1 and S2,† respectively. Transition temperatures were determined from the second round of DSC heating scans. The values of T_g for **PT*t*TPA**, **PBT*t*TPA**, **PT*t*Cz**, and **PBT*t*Cz** were 112, 104, 121, and 115 °C, respectively, which are suitable for PSC applications. A single endothermic glass transition was observed for each conjugated copolymer, implying that the 2-ethylhexyl-substituted thiophene derivative-based conjugated units (T and BT) and electron-donating bulky pendants (*t*Cz and *t*TPA) were distributed homogeneously. Moreover, the T_g values of BT-based copolymers (**PBT*t*TPA** and **PBT*t*Cz**) were lower than those of the T-based copolymers (**PT*t*TPA** and **PT*t*Cz**), presumably because of the presence of a higher content of 2-ethylhexyl chains in **PBT*t*TPA** and **PBT*t*Cz**. Furthermore, higher T_g values were observed for the *t*Cz-containing PTs (**PT*t*Cz** and **PBT*t*Cz**) as compared to the *t*TPA-containing PTs (**PT*t*TPA** and **PBT*t*TPA**). The reason for this may be that the propeller-shaped conformation of the TPA moiety is expected to increase the free volume between the polymer chains, while the coplanar structure of carbazole permits a higher packing density.[34] The values of T_d for **PT*t*TPA**, PTBT*t*PA, **PT*t*Cz**, and **PBT*t*Cz** were 414, 416, 418, and 421 °C, respectively.

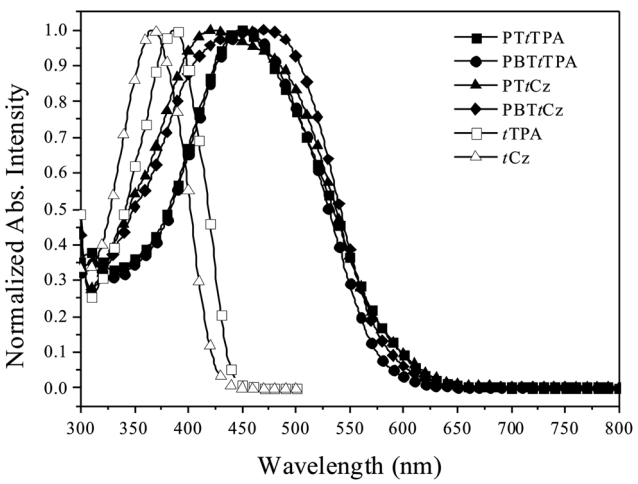

Fig. 2 Normalized UV-vis absorption spectra of aromatic amine pendants and PTs in *o*-DCB solutions.

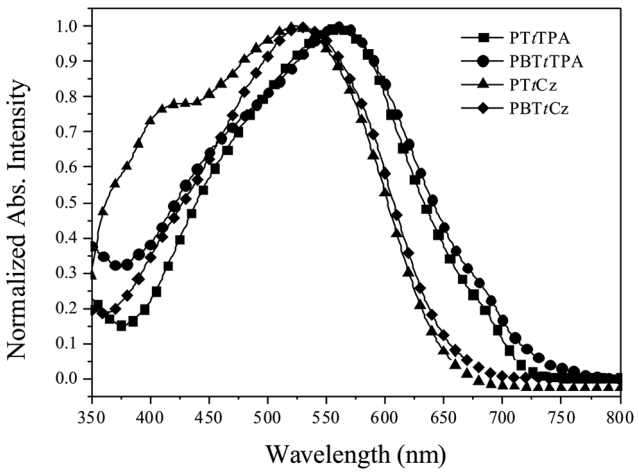

Fig. 3 Normalized UV-vis absorption spectra of aromatic amine pendants and PTs in thin films.

3.2 Optical properties of PTs

The normalized UV-vis absorption spectra of the PTs in *o*-DCB solution and as solid films are shown in Fig. 2 and 3 (see ESI†). Table 1 summarizes the photophysical properties of the copolymers. As shown in Fig. 2, the absorption bands of the PTs in *o*-DCB ranged from 325 to 650 nm, and each polymer showed a single broad absorption band. The maximum absorption wavelengths of conjugated pendants *t*TPA and *t*Cz in *o*-DCB were at 385 nm and 373 nm, respectively. The red-shift of the absorption band for *t*TPA relative to *t*Cz should be due to the stronger electron-donating character and more efficient π–π* charge transfer of *t*TPA. In general, PTs functionalized with conjugated pendants exhibit two maximum absorption peaks, one in the visible region attributed to the π–π* transition of the conjugated polymer main chains, and the other in the UV region attributed to the conjugated side chains.[35] The fact that our PTs functionalized with conjugated *t*TPA or *t*Cz moieties showed only a single broad absorption peak indicates a high degree of intramolecular conjugation within the conjugated frameworks of the polymers in solution. However, the full widths at half-maximum of **PT*t*Cz** and **PBT*t*Cz** were much greater than those of **PT*t*TPA** and **PBT*t*TPA**, and the absorption intensities of **PT*t*Cz** and **PBT*t*Cz** at 325–425 nm were much higher than those of the **PT*t*TPA** and **PBT*t*TPA**. This implies poorer coplanarity and less effective conjugation between the polymer backbone and conjugated pendants in the *t*Cz-containing polymers as compared to the *t*TPA-containing polymers. In addition, **PBT*t*Cz** has a longer conjugation length and greater π-electron delocalization along the polymer backbone than **PT*t*Cz**, and this is reflected in a red-shift of the absorption band for **PBT*t*Cz** as compared to that of **PT*t*Cz**. However, the effect of the BT unit on the UV-vis absorption was less marked for *t*TPA pendant polymers as compared with *t*Cz pendant polymers.

As shown in Fig. 3, the absorption bands of **PT*t*TPA** and **PBT*t*TPA** thin films ranged from 350 to 750 nm, while the absorption bands of **PT*t*Cz** and **PBT*t*Cz** thin films ranged from 350 to 700 nm. The red-shifts and full widths at half-maximum

of the absorption bands of the copolymers in the films were greater than those in solution, presumably because of strong noncovalent interactions (*e.g.*, π–π stacking) between the polymer chains arising from the high degree of coplanarity of the polymer backbone and conjugated pendants. Thus, loss of planar π-conjugation owing to twisting of the main chain in the presence of bulky moieties was suppressed by the incorporation of rigid conjugation units (T and BT) into the polymer backbone. It is interesting to note that there was an absorption shoulder in the near-UV region in the case of **PT*t*Cz** film, which might be caused by the twisting of bulky *t*Cz pendants out of the π–π conjugation plane. However, the absorption of *t*Cz pendants in the near-UV region was suppressed in the **PBT*t*Cz** film. This suggests that the presence of BT in the polymer backbone was more effective than that of T to reduce the steric hindrance among conjugated pendants and extend the π-conjugation.

We determined the band-gap energies (E_g) of the conjugated polymers in the thin film state from the onset wavelengths of their absorption bands. As shown in Table 1, the values of E_g for **PT*t*TPA**, **PBT*t*TPA**, **PT*t*Cz**, and **PBT*t*Cz** were 1.65, 1.58, 1.80, 1.77 eV, respectively. The lower values of E_g of **PT*t*TPA** and **PBT*t*TPA** should reflect higher charge transfer between the polymer backbone and conjugated pendants for the *t*TPA pendant polymers as compared to the *t*Cz pendant polymers. In addition, BT-containing **PBT*t*TPA** and **PBT*t*Cz** have a longer conjugation length and greater π-electron delocalization along the polymer backbone than T-containing **PT*t*TPA** and **PT*t*Cz**, and these factors may contribute to the lower values of E_g. Generally, broader absorption and lower band-gap energy characteristics are expected to improve the solar-light absorption efficiency of the photo-energy conversion layer in PSCs, resulting in larger photocurrent generation.

The photoluminescence (PL) emission spectra of PTs as thin films are shown in Fig. 4. PTs exhibited PL maxima at *ca.* 658–664 nm (red region) upon excitation at 350 nm. *t*TPA pendant polymers (**PT*t*TPA** and **PBT*t*TPA**) showed a red-shift of the emission band relative to the *t*Cz pendant polymers (**PT*t*Cz** and **PBT*t*Cz**) due to the stronger electron-donating ability of *t*TPA pendants. The PL emission of a thin film of the **PT*t*TPA**/$PC_{61}BM$ (w/w = 1 : 1) blend is also shown in Fig. 4. The PL emission was almost completely quenched by the addition of $PC_{61}BM$ (w/w = 1 : 1) to **PT*t*TPA**. Similar quenching was also observed for **PBT*t*TPA**, **PT*t*Cz**, and **PBT*t*Cz**. The highly efficient quenching suggests that excitons generated by absorbed photons dissociated almost completely to free charge carriers (electrons and holes). Thus, effective charge transfer from the conjugated copolymer to the electron acceptor $PC_{61}BM$ takes place—a basic requirement for preparing PSCs that exhibit satisfactory PV performance.[36]

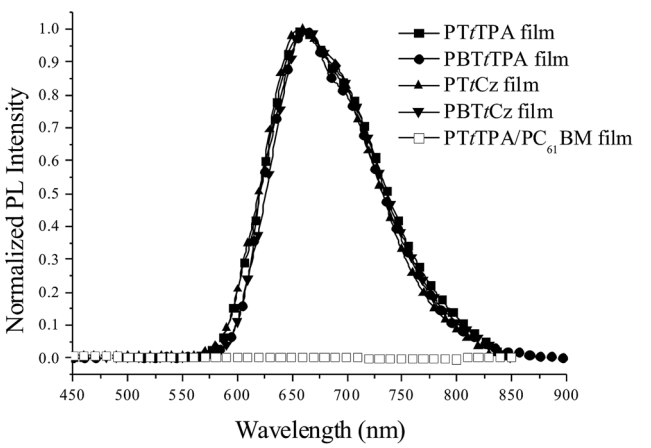

Fig. 4 Normalized PL spectra of PTs in thin films.

3.3 Electrochemical properties of PTs

Since the PV performance of PSCs is related to the electrochemical behavior of the conjugated polymer, we employed cyclic voltammetry to investigate the electrochemical behavior of our PTs and to estimate the energy levels of the highest occupied molecular orbital (HOMO). The oxidation behaviors in the CV curves of the PTs are shown in Fig. 5. The electrochemical properties of the copolymers are summarized in Table 1. The oxidation potentials (E_{on}^{ox}) of **PT*t*TPA**, **PBT*t*TPA**, **PT*t*Cz**, and **PBT*t*Cz** were 0.42, 0.40, 0.45, and 0.43 V, respectively. From these values, the HOMO levels of the copolymers were calculated according to the following equation:

$$\mathrm{HOMO} = -e(E_{on}^{ox} - E_{on,ferrocene}^{ox} + 4.8)\ (\mathrm{eV})$$

where 4.80 eV is the energy level of ferrocene below the vacuum level and the E_{on}^{ox} of ferrocene/ferrocene$^+$ is 0.09 V in 0.1 M Bu_4NClO_4–MeCN solution. The HOMO levels were obtained as −5.13, −5.11, −5.16 and −5.14 eV for **PT*t*TPA**, **PBT*t*TPA**, **PT*t*Cz**, and **PBT*t*Cz**, respectively. The HOMO levels of *t*TPA pendant polymers are higher than those of TPA pendant polymers.[21] It is also known that attachment of *tert*-butyl groups on electrochemically active sites of aromatic amines leads to a decrease of the HOMO level.[37] Here, the *t*TPA pendant polymers (**PT*t*TPA**

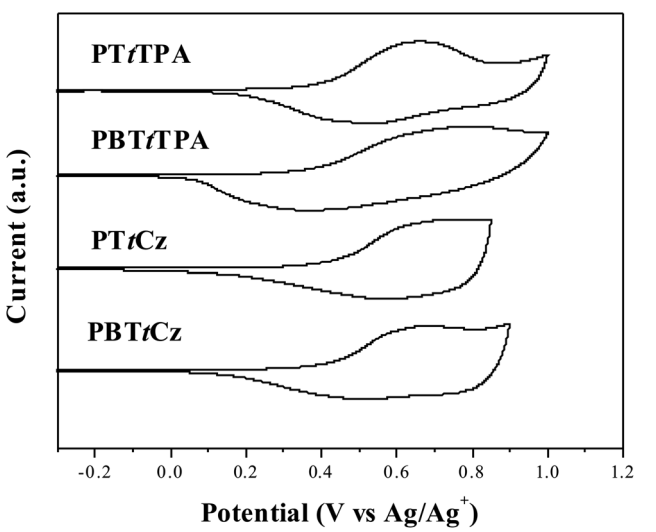

Fig. 5 Cyclic voltammograms of PTs films on platinum plates in acetonitrile solution of 0.1 mol L^{-1} of Bu_4NClO_4.

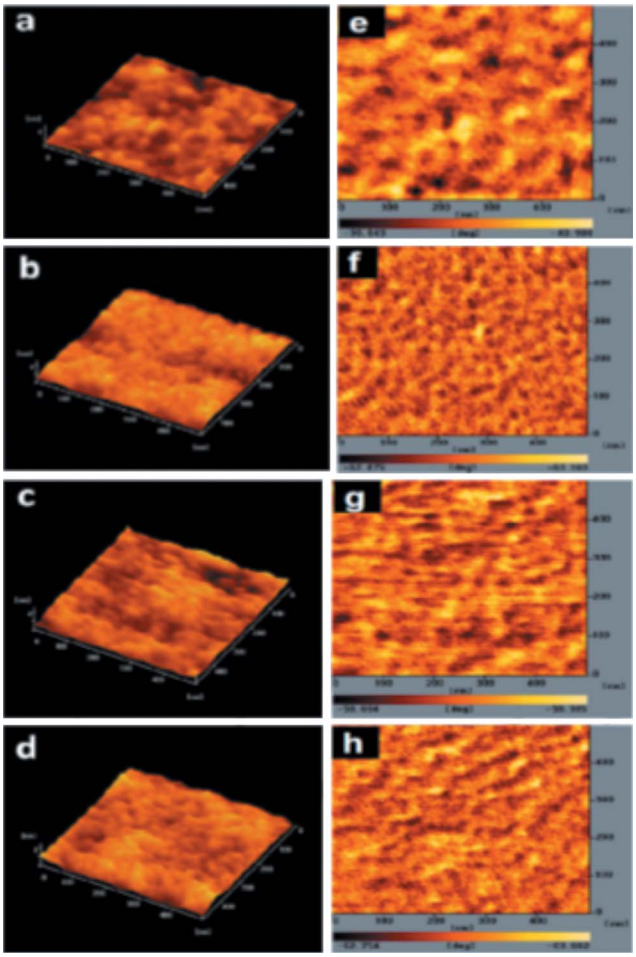

Fig. 6 AFM tapping mode topographic (a–d) and phase (e–h) images of **PT*t*TPA** (a and e), **PBT*t*TPA** (b and f), **PT*t*Cz** (c and g), and **PBT*t*Cz** (d and f). The area was 1 μm × 1 μm.

and **PBT*t*TPA**) exhibited higher HOMO levels than *t*Cz pendant polymers (**PT*t*Cz** and **PBT*t*Cz**), presumably because of the lower oxidation potential and weaker electron-donating ability of carbazole derivatives.[38] Further, **PBT*t*TPA** and **PBT*t*Cz** are expected to have higher HOMO levels than **PT*t*TPA** and **PT*t*Cz** because of the longer conjugation length and π-electron delocalization in BT-based polymers compared to T-based polymers. Because no reversible n-doping process was observed in the CV spectra, the LUMO levels were estimated from the HOMO levels and UV-vis absorption E_g using the equation:

$$\text{LUMO} = (\text{HOMO} + E_g)\ (\text{eV})$$

The LUMO levels were obtained as −3.48 eV for **PT*t*TPA**, −3.53 eV for **PBT*t*TPA**, −3.36 eV for **PT*t*Cz**, and −3.37 eV for **PBT*t*Cz**. Clearly, the electrochemical properties of these PTs can be tuned by incorporating thiophene units with different conjugation lengths (T and BT) into the polymer backbone and attaching different electron-donating pendants (*t*TPA and *t*Cz). In general, the HOMO energy level of a p-type conjugated polymer is an important parameter affecting the performance of BHJ-type cells. High open circuit voltages (V_{oc}) are typically obtained for PSCs fabricated from conjugated polymers with low HOMO energy levels.[39]

3.4 Morphology of thin films of PT/$PC_{61}BM$ blends

The performance of PSCs is strongly dependent on the morphology of the conjugated polymer/fullerene derivative composite film. To avoid recombination of excitons, the P/N heterojunction phase must be controlled at the nanoscale level. This is because the diffusion range of the exciton is approximately 3–10 nm.[40,41] We used AFM microscopy to investigate the compatibility and morphology of our conjugated polymer/$PC_{61}BM$ composite films. Fig. 6 displays topographic and phase-contrast images of the **PT*t*TPA**/$PC_{61}BM$, **PBT*t*TPA**/$PC_{61}BM$, **PT*t*Cz**/$PC_{61}BM$, and **PBT*t*Cz**/$PC_{61}BM$ films (w/w = 1 : 1) after annealing at 110 °C for 10 min. In each case, we observed a phase-separated interpenetrating network with sizable $PC_{61}BM$ domains. Some degree of phase separation is critical for efficient formation of free carriers to provide optimal PV properties

Table 2 Photovoltaic performance of PSCs of conventional structure prepared with PT/$PC_{61}BM$ photoactive layers[a]

PSC	Photoactive layer	PT/$PC_{61}BM$ (w/w)	d (nm)	R (nm)	V_{oc} (V)	J_{sc} (mA cm^{-2})	FF	η (%)
PSC I-1	**PT*t*TPA**/$PC_{61}BM$	1 : 1	115	0.24	0.70	8.12	0.31	1.76
PSC I-2	**PT*t*TPA**/$PC_{61}BM$	1 : 2	112	0.28	0.67	10.73	0.31	2.23
PSC I-3	**PT*t*TPA**/$PC_{61}BM$	1 : 3	109	0.37	0.68	10.90	0.34	2.52
PSC I-4	**PT*t*TPA**/$PC_{61}BM$	1 : 4	101	0.35	0.60	12.10	0.30	2.18
PSC II-1	**PBT*t*TPA**/$PC_{61}BM$	1 : 1	106	0.27	0.69	8.78	0.32	1.94
PSC II-2	**PBT*t*TPA**/$PC_{61}BM$	1 : 2	102	0.30	0.68	9.31	0.38	2.40
PSC II-3	**PBT*t*TPA**/$PC_{61}BM$	1 : 3	98	0.26	0.70	9.60	0.39	2.62
PSC II-4	**PBT*t*TPA**/$PC_{61}BM$	1 : 4	92	0.32	0.66	9.65	0.38	2.42
PSC III-1	**PT*t*Cz**/$PC_{61}BM$	1 : 1	112	0.30	0.79	7.21	0.30	1.71
PSC III-2	**PT*t*Cz**/$PC_{61}BM$	1 : 2	109	0.29	0.76	10.17	0.31	2.40
PSC III-3	**PT*t*Cz**/$PC_{61}BM$	1 : 3	105	0.28	0.74	10.69	0.35	2.77
PSC III-4	**PT*t*Cz**/$PC_{61}BM$	1 : 4	98	0.32	0.70	10.93	0.35	2.68
PSC IV-1	**PBT*t*Cz**/$PC_{61}BM$	1 : 1	110	0.28	0.74	8.01	0.31	1.84
PSC IV-2	**PBT*t*Cz**/$PC_{61}BM$	1 : 2	108	0.32	0.65	9.16	0.36	2.14
PSC IV-3	**PBT*t*Cz**/$PC_{61}BM$	1 : 3	102	0.29	0.64	9.88	0.37	2.34
PSC IV-4	**PBT*t*Cz**/$PC_{61}BM$	1 : 4	95	0.38	0.60	9.45	0.33	1.87

[a] d: thickness of the photo-active layer. R: roughness of the photo-active layer.

of PSCs. The phase-contrast images indicated that the $PC_{61}BM$ domains in the **PBT*t*TPA**/$PC_{61}BM$ film were smaller than those in the **PT*t*TPA**/$PC_{61}BM$ film, implying better compatibility between the conjugated polymer and $PC_{61}BM$ in the case of **PBT*t*TPA**. This can be attributed to the lower *t*TPA pendant content of **PBT*t*TPA**, which should permit easier incorporation of $PC_{61}BM$ into the polymer chains. However, the difference between the phase-contrast images of **PT*t*Cz**/$PC_{61}BM$ and **PBT*t*Cz**/$PC_{61}BM$ films was less marked than that between **PT*t*TPA**/$PC_{61}BM$ and **PBT*t*TPA**/$PC_{61}BM$ films. The surface roughness of our PT/$PC_{61}BM$ films was in the range of 0.24–0.38 nm (Table 2), which is lower than that reported for films prepared with PT containing linear alkyl chain substitution.[21] These results indicated that the compatibility and surface morphology of the PT/$PC_{61}BM$ film are influenced by the chemical structure of the alkyl side-chains of PT (branched 2-ethylhexyl in our case).[42,43] In order to further study the composition effect on the morphology of PT/$PC_{61}BM$ films, phase-contrast images of the **PT*t*TPA**/$PC_{61}BM$, **PBT*t*TPA**/$PC_{61}BM$, **PT*t*Cz**/$PC_{61}BM$, and **PBT*t*Cz**/$PC_{61}BM$ films (w/w = 1 : 3 and 1 : 4) were taken after annealing the samples at 110 °C for 10 min and are displayed in Fig. 7. The phase-contrast of the PT/$PC_{61}BM$ films was more obviously due to the incorporation of a higher content of $PC_{61}BM$. However, the distribution of the $PC_{61}BM$ units in the polymers was uniform for the **PT*t*TPA**/$PC_{61}BM$ and **PBT*t*TPA**/$PC_{61}BM$ films. In addition, the distribution of the $PC_{61}BM$ units in the *t*Cz pendant polymers (**PT*t*Cz** and **PBT*t*Cz**) was less uniform as compared to that of the *t*TPA pendant polymer/$PC_{61}BM$ films, especially for the blend films with higher PC61BM contents (Fig. 7(f) and (h)). This implies that the compatibility between the *t*TPA pendant polymers and $PC_{61}BM$ was better than that of the *t*Cz pendant polymers and $PC_{61}BM$. Moreover, a more homogeneous morphology was observed in **PT*t*Cz**/$PC_{61}BM$ films (Fig. 7(e) and (f)) in comparison with that of the **PBT*t*Cz**/$PC_{61}BM$ films (Fig. 7(g) and (h)). This is because **PT*t*Cz** exhibits a higher grafting content of 2-ethylhexyl groups than the **PBT*t*Cz** sample. The higher grafting content of 2-ethylhexyl groups would enhance the compatibility between the **PT*t*Cz** and $PC_{61}BM$.

In order to further characterize the distribution of $PC_{61}BM$ in PT/$PC_{61}BM$ films, TEM investigation was carried out.[44] Bright-field (BF) TEM images of **PT*t*TPA**/$PC_{61}BM$, **PBT*t*TPA**/$PC_{61}BM$, **PT*t*Cz**/$PC_{61}BM$, and **PBT*t*Cz**/$PC_{61}BM$ films (w/w = 1 : 1) are shown in Fig. 8. The dark areas in the images represent $PC_{61}BM$ domains, because the electron-scattering density of $PC_{61}BM$ is greater than that of the conjugated polymer.[45] As shown in Fig. 8(a), nanometer-scale clusters of $PC_{61}BM$ were present in the **PT*t*TPA**/$PC_{61}BM$ film. In contrast, a more homogeneous morphology was seen in the **PBT*t*TPA**/$PC_{61}BM$ film (Fig. 8(b)), presumably because

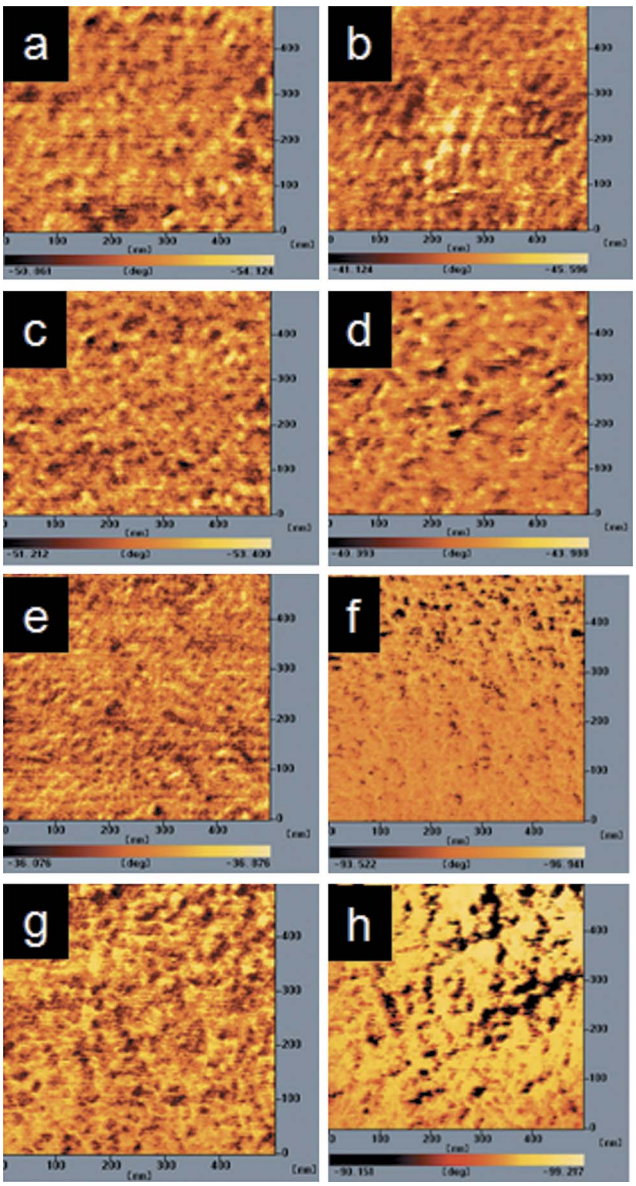

Fig. 7 Phase-contrast images of the **PT*t*TPA**/$PC_{61}BM$ (a and b), **PBT*t*TPA**/$PC_{61}BM$ (c and d), **PT*t*Cz**/$PC_{61}BM$ (e and f), and **PBT*t*Cz**/$PC_{61}BM$ (g and h) films (a, c, e, and g: w/w = 1 : 3; b, d, f, and h: w/w = 1 : 4) after annealing at 110 °C for 10 min.

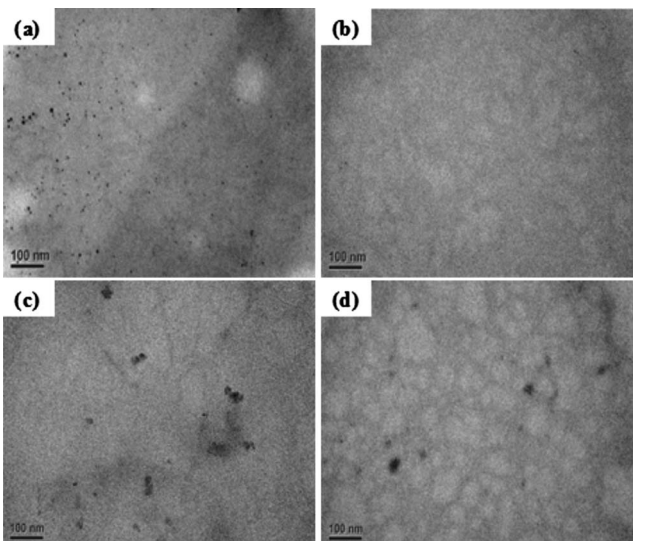

Fig. 8 TEM images of PTs/$PC_{61}BM$ (w/w = 1 : 1) blend films: (a) **PT*t*TPA**, (b) **PBT*t*TPA**(c) **PT*t*Cz**, and (d) **PBT*t*Cz**.

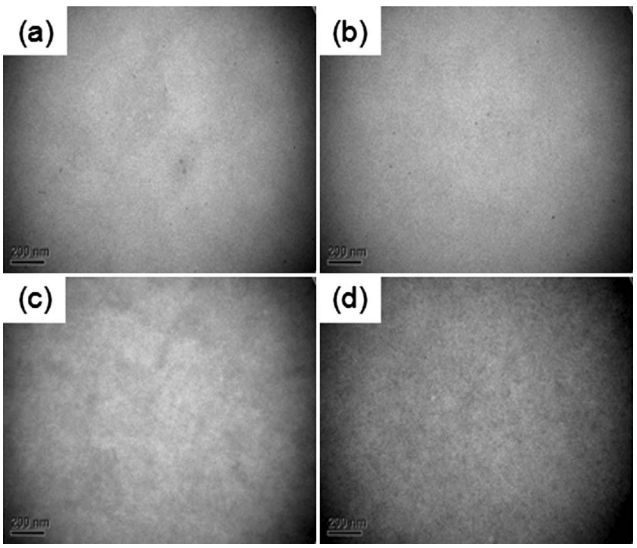

Fig. 9 TEM images of PTs/$PC_{61}BM$ (w/w = 1 : 3) blend films: (a) **PT*t*TPA**, (b) **PBT*t*TPA** (c) **PT*t*Cz**, and (d) **PBT*t*Cz**.

the lower content of pendant *t*TPA provides sufficient free volume for easy incorporation of $PC_{61}BM$ into the polymer chains, so that phase separation and crystallization of $PC_{61}BM$ are suppressed. As shown in Fig. 8(c), the TEM image of the **PT*t*Cz**/$PC_{61}BM$ blend film revealed $PC_{61}BM$ clusters about several tens of nanometers in size, considerably larger than in the case of the **PT*t*TPA**/$PC_{61}BM$ film (Fig. 8(a)). The closer packing of *t*Cz pendants presumably reduced the compatibility between the polymer and $PC_{61}BM$ in the film.[34] In addition, TEM images revealed several $PC_{61}BM$ clusters in the **PBT*t*Cz**/$PC_{61}BM$ film (Fig. 8(d)). The compatibility between the polymer and $PC_{61}BM$ in the **PBT*t*Cz**/$PC_{61}BM$ film was similar to that of the **PT*t*Cz**/$PC_{61}BM$ film. It is noteworthy that some bright domains corresponding to higher-order packing of polymer chains can be seen in **PBT*t*TPA**/$PC_{61}BM$ and **PBT*t*Cz**/$PC_{61}BM$ films (Fig. 8(b) and (d)). Furthermore, TEM images of **PT*t*TPA**/$PC_{61}BM$, **PBT*t*TPA**/$PC_{61}BM$, **PT*t*Cz**/$PC_{61}BM$, and **PBT*t*Cz**/$PC_{61}BM$ films (w/w = 1 : 3) are shown in Fig. 9. TEM images indicate that the distribution of the $PC_{61}BM$ units in the *t*TPA pendant polymer/$PC_{61}BM$ film was more uniform than that of the $PC_{61}BM$ units in the *t*Cz pendant polymers (**PT*t*Cz** and **PBT*t*Cz**)/$PC_{61}BM$ film. Poor compatibility between the polymer and $PC_{61}BM$ was observed for the **PBT*t*Cz**/$PC_{61}BM$ film, which was attributed to a lower grafting content of 2-ethylhexyl groups of **PBT*t*Cz**. Notably, the bright domains corresponding to higher-order packing of polymer chains were vanished in **PBT*t*TPA**/$PC_{61}BM$ and **PBT*t*Cz**/$PC_{61}BM$ films (Fig. 9(b) and (d)), due to the incorporation of high content of $PC_{61}BM$.

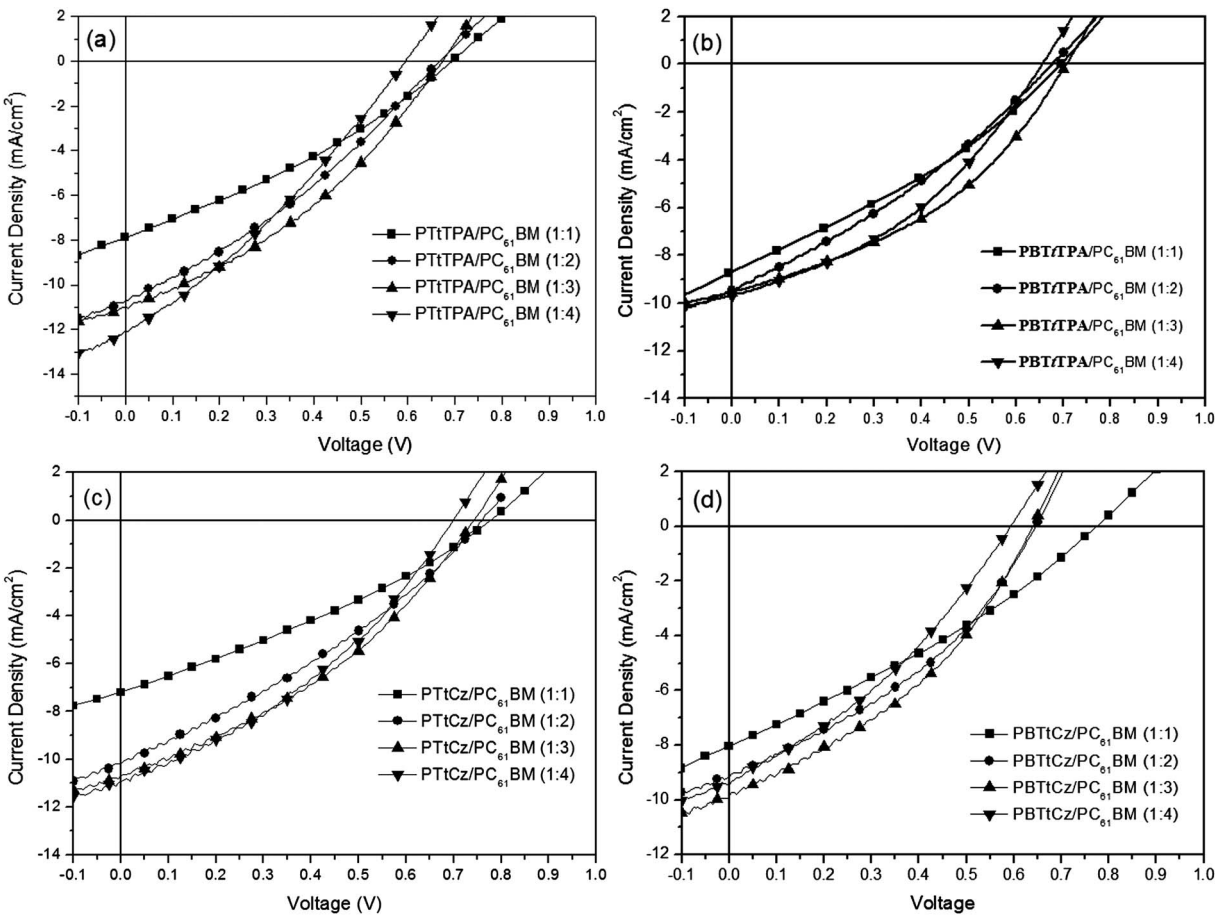

Fig. 10 Current density–potential characteristics of illuminated (AM 1.5G, 100 mW cm^{-2}) PTs/$PC_{61}BM$-based solar cells.

3.5 PV properties of PSCs based on PT/$PC_{61}BM$ films

We fabricated PSCs by incorporating a photoactive layer of the PT/$PC_{61}BM$ blend prepared by means of an optimized spin-coating procedure. Fig. 10 shows photocurrent density–voltage plots of the PSCs. Table 2 summarizes the PV properties of these PSCs, including V_{oc}, J_{sc}, fill factor (FF), and η values. For the **PT*t*TPA**/$PC_{61}BM$-based PSCs (PSC I-1–PSC I-4), the V_{oc} value decreased with increasing $PC_{61}BM$ content. The band gap energy of a polymer/$PC_{61}BM$ film is, however, affected by the $PC_{61}BM$ content because charge transfer occurs between the polymer and $PC_{61}BM$. The band gap energies of the polymer/$PC_{61}BM$ blend films decreased slightly upon increasing the $PC_{61}BM$ content; consequently, the values of V_{oc} decreased slightly upon increasing the $PC_{61}BM$ content.[46] Moreover, the J_{sc}, FF, and η values of PSCs increased upon increasing the $PC_{61}BM$ content. The highest J_{sc}, FF, and η values were observed for the PSC I-3. This indicates that the optimal composition of **PT*t*TPA** and $PC_{61}BM$ was about 1 : 3 (w/w) for the **PT*t*TPA** based PSCs. Higher concentrations of $PC_{61}BM$ favored the formation of phase-separated interpenetrating networks with sizable domains in the photoactive layer, which in turn led to an effective charge separation.[46] However, the excessive incorporation of the $PC_{61}BM$ content was not favorable for the PV performance of PSCs. PSC I-4 shows poorer PV performance than PSC I-2 and PSC I-3. As summarized in Table 2, a higher content of the $PC_{61}BM$ resulted in a smaller thickness of the polymer/$PC_{61}BM$ film, especially for the photoactive layer of PSC I-4. A smaller thickness led to the higher current leakage of PSC, subsequently, poorer PV performance was observed for PSC I-4. For the **PBT*t*TPA**/$PC_{61}BM$-based PSCs (PSC II-1–PSC II-4), the V_{oc} values were comparable with those of the **PT*t*TPA**/$PC_{61}BM$-based PSCs, even though the HOMO level of **PBT*t*TPA** was slightly higher than that of the **PT*t*TPA**. In addition, the FF and η values of **PBT*t*TPA**/$PC_{61}BM$-based PSCs were better than those of the **PT*t*TPA**/$PC_{61}BM$-based PSCs, while the J_{sc} values behaved otherwise. We attribute the larger values of FF and η of **PBT*t*TPA**/$PC_{61}BM$-based PSCs to better conjugation and broader absorption of the **PBT*t*TPA**. In contrast, lower *t*TPA content led to the lower absorption intensity of **PBT*t*TPA**, which resulted in lower J_{sc} values of **PBT*t*TPA**/$PC_{61}BM$-based PSCs. In addition, the values of V_{oc} of the **PT*t*Cz**/$PC_{61}BM$ based PSCs (PSC III-1–PSC III-4) were larger than those of the **PT*t*TPA**/$PC_{61}BM$- and **PBT*t*TPA**/$PC_{61}BM$-based PSCs, respectively, presumably because of the lower HOMO level of **PT*t*Cz** as compared to those of **PT*t*TPA** and **PBT*t*TPA**. The J_{sc} and FF values of **PT*t*Cz**/$PC_{61}BM$ based PSCs were comparable to those of the **PT*t*TPA**/$PC_{61}BM$- and **PBT*t*TPA**/$PC_{61}BM$-based PSCs. Higher V_{oc} values resulted in the larger η values of the **PT*t*Cz**/$PC_{61}BM$ based PSCs in comparison with those of the **PT*t*TPA**/$PC_{61}BM$- and **PBT*t*TPA**/$PC_{61}BM$-based PSCs. On the other hand, the **PBT*t*Cz**/$PC_{61}BM$ based PSCs (PSC IV-1–PSC IV-4) showed poorer PV performance as compared to **PT*t*TPA**/$PC_{61}BM$-, **PBT*t*TPA**/$PC_{61}BM$-, and **PT*t*Cz**/$PC_{61}BM$-based PSCs. As shown in Fig. 7(g) and 7(h), poor compatibility between the polymer and $PC_{61}BM$ was observed for the **PBT*t*Cz**/$PC_{61}BM$ film. The microphase separation and aggregation of $PC_{61}BM$ resulted in the charge recombination and current leakage, which would decrease V_{oc}, J_{sc}, FF, and η values of the **PBT*t*Cz**/$PC_{61}BM$-based PSCs.

4 Conclusion

We synthesized a series of low-band-gap PTs featuring conjugated T and BT units in the polymer backbone with conjugated *t*TPA and *t*Cz moieties as pendant units, and evaluated their structure and photophysical and electrochemical properties. Incorporation of T and BT into the polymer backbone of PTs with bulky pendant groups is expected to reduce the steric hindrance between adjacent pendants and therefore to enhance the coplanarity of the polymer backbone and pendants. Indeed, efficient intramolecular conjugation within the conjugated frameworks of the polymers was apparent in terms of lower band-gap energies. Therefore, the **PBT*t*TPA**/PC61BM-based PSCs showed superior photovoltaic performance to the **PT*t*TPA**/$PC_{61}BM$-based PSCs. However, the PV performance was not solely dependent on the intramolecular conjugation or band-gap energy of the polymer. Highest values of V_{oc}, J_{sc}, and η were observed for the **PT*t*Cz**/$PC_{61}BM$-based PSCs, even though the *t*TPA pendant polymers exhibit higher electron-donating ability, broader UV-vis absorption band, and lower band-gap energy than the *t*Cz pendant polymers. This is attributed to the lower HOMO level and higher conjugated side-chain content of **PT*t*Cz**. In addition, the morphology of the polymer and $PC_{61}BM$ is another important issue in the PV performance of PSCs. The aggregation of $PC_{61}BM$ resulted in the charge recombination and current leakage, which would decrease the V_{oc}, J_{sc}, FF, and η values of **PBT*t*Cz**/$PC_{61}BM$-based PSCs. Finally, we found that the performance of PT/$PC_{61}BM$-based PSCs was dependent on not only the intramolecular conjugation and absorption band broadness of the polymer, but also the HOMO level of the polymer and photoactive layer quality.

Acknowledgements

We thank the National Science Council (NSC) and the Ministry of Education, Taiwan, for financial support under the ATU plan.

References

1 R. D. McCullough, *Adv. Mater.*, 1998, **10**, 93.
2 R. D. McCullough, in *Handbook of Oligo- and Polythiophenes*, ed. D. Fichou, Wiley-VCH, 2007, p. 1.
3 I. F. Perepichka, D. F. Perepichka, H. Meng and F. Wudl, *Adv. Mater.*, 2005, **17**, 2281.
4 Y. Wang, E. Zhou, Y. Liu, H. Xi, S. Ye, W. Wu, Y. Guo, C. A. Di, Y. Sun, G. Yu and Y. Li, *Chem. Mater.*, 2007, **19**, 3361.
5 C. Y. Yu, B. T. Ko, C. Ting and C. P. Chen, *Sol. Energy Mater. Sol. Cells*, 2009, **93**, 613.
6 M. Manceau, D. Angmo, M. Jorgensen and F. C. Krebs, *Org. Electron.*, 2011, **12**, 566.
7 M. Zhang, X. Guo, Y. Yang, J. Zhang, Z. G. Zhang and Y. Li, *Polym. Chem.*, 2011, **2**, 2900.
8 K. S. Chen, Y. Zhang, H. L. Yip, Y. Sun, J. A. Davies, C. Ting, C. P. Chen and A. K. Y. Jen, *Org. Electron.*, 2011, **12**, 794.
9 P. T. Wu, G. Ren and S. A. Jenekhe, *Macromolecules*, 2010, **43**, 3306.

10 G. Ren, P. T. Wu and S. A. Jenekhe, *Chem. Mater.*, 2010, **22**, 2020.
11 S. Gunes, H. Neugebauer and N. S. Sariciftci, *Chem. Rev.*, 2007, **107**, 1324.
12 C. Winder and N. S. Sariciftci, *J. Mater. Chem.*, 2004, **14**, 1077.
13 C. H. Woo, B. C. Thompson, B. J. Kim, M. F. Toney and J. M. J. Fréchet, *J. Am. Chem. Soc.*, 2008, **130**, 16324.
14 C. Duan, K. S. Chen, F. Huang, H. L. Yip, S. Liu, J. Zhang, A. K. Y. Jen and Y. Cao, *Chem. Mater.*, 2010, **22**, 6444.
15 Y. Zou, G. Sang, W. Wu, Y. Liu and Y. Li, *Synth. Met.*, 2009, **159**, 182.
16 Y. Li, H. Xia, B. Xu, S. Wen and W. Tian, *J. Polym. Sci., Part A: Polym. Chem.*, 2008, **46**, 3970.
17 Y. T. Chang, S. L. Hsu, M. H. Su and K. H. Wei, *Adv. Mater.*, 2009, **21**, 2093.
18 Z. G. Zhang, S. Y. Zhang, J. Min, C. H. Chui, J. Zhang, M. J. Zhang and Y. F. Li, *Macromolecules*, 2012, **45**, 113.
19 J. H. Tsai, W. Y. Lee, W. C. Chen, C. Y. Yu, G. W. Hwang and C. Ting, *Chem. Mater.*, 2010, **22**, 3290.
20 Z. Gu, P. Shen, S. W. Tsang, Y. Tao, B. Zhao, P. Tang, Y. Nie, Y. Fang and S. Tan, *Chem. Commun.*, 2011, **47**, 9381.
21 H. J. Wang, L. H. Chan, C. P. Chen, S. L. Lin, R. H. Lee and R. J. Jeng, *Polymer*, 2011, **52**, 326.
22 J. Hou, Z. Tan, Y. Yan, Y. He, C. Yang and Y. Li, *J. Am. Chem. Soc.*, 2006, **128**, 4911.
23 J. Hou, L. Huo, C. He, C. Yang and Y. Li, *Macromolecules*, 2006, **39**, 594.
24 G. Y. Sang, E. J. Zhou, Y. Huang, Y. P. Zou, G. J. Zhao and Y. F. Li, *J. Phys. Chem. C*, 2009, **113**, 5879.
25 W. W. Li, Y. Han, Y. L. Chen, C. H. Li, B. S. Li and Z. S. Bo, *Macromol. Chem. Phys.*, 2010, **211**, 948.
26 H. J. Wang, L. H. Chan, C. P. Chen, R. H. Lee, W. C. Su and R. J. Jeng, *Thin Solid Films*, 2011, **519**, 5264.
27 K. Colladet, S. Fourier, T. J. Cleij, L. Lutsen, J. Gelan, D. Vanderzande, L. Huong Nguyen, H. Neugebauer, S. Sariciftci, A. Aguirre, G. Janssen and E. Goovaerts, *Macromolecules*, 2007, **40**, 65.
28 Z. G. Zhang, S. Zhang, J. Min, C. Chui, J. Zhang, M. Zhang and Y. Li, *Macromolecules*, 2012, **45**, 113.
29 Z. G. Zhang, S. Zhang, J. Min, C. Cui, H. Geng, Z. Shuai and Y. Li, *Macromolecules*, 2012, **45**, 2312.
30 X. Yang, R. Lu, T. Xu, P. Xue, X. Liu and Y. Zhao, *Chem. Commun.*, 2008, 453.
31 Y. Zhang, K. Tajima, K. Hirota and K. Hashimoto, *J. Am. Chem. Soc.*, 2008, **130**, 7812.
32 B. Tsuie, J. L. Reddinger, G. A. Sotzing, J. Soloducho, A. R. Katritzky and J. R. Reynolds, *J. Mater. Chem.*, 1999, **9**, 2189.
33 C. P. Chen, S. H. Chan, T. C. Chao, C. Ting and B. T. Ko, *J. Am. Chem. Soc.*, 2008, **130**, 12828.
34 G. S. Liou, S. H. Hsiao and H. W. Chen, *J. Mater. Chem.*, 2006, **16**, 1831.
35 Y. Li and Y. Zou, *Adv. Mater.*, 2008, **20**, 2952.
36 M. A. Ibrahim, H. K. Roth, U. Zhokhavets, G. Gobsch and S. Sensfuss, *Sol. Energy Mater. Sol. Cells*, 2005, **85**, 13.
37 H. M. Wang, S. H. Hsiao, G. S. Liou and C. H. Sun, *J. Polym. Sci., Part A: Polym. Chem.*, 2010, **48**, 4775.
38 O. Kwon, S. Barlow, S. A. Odom, L. Beverina, N. J. Thompson, E. Zojer, J. L. Brédas and S. R. Marder, *J. Phys. Chem. A*, 2005, **109**, 9346.
39 M. C. Scharber, D. Wuhlbacher, M. Koppe, P. Denk, C. Waldauf, A. J. Heeger and C. L. Brabec, *Adv. Mater.*, 2006, **18**, 789.
40 A. C. Mayer, S. R. Scully, B. E. Hardin, M. W. Rowell and M. D. McGehee, *Mater. Today*, 2007, **10**, 28.
41 F. Yang, M. Shtein and S. R. Forrest, *Nat. Mater.*, 2005, **4**, 37.
42 Y. Liang, D. Feng, Y. Wu, S. T. Tsai, G. Li, C. Ray and L. Yu, *J. Am. Chem. Soc.*, 2009, **131**, 7792.
43 G. Adam, A. Pivrikas, A. M. Ramil, S. Tadesse, T. Yohannes, N. S. Sariciftci and D. A. M. Egbe, *J. Mater. Chem.*, 2011, **21**, 2594.
44 S. S. van Bavel, M. Bärenklau, G. de With, H. Hoppe and J. Loos, *Adv. Funct. Mater.*, 2010, **20**, 1458.
45 X. Yang, J. K. J. van Duren, R. A. J. Janssen, M. A. J. Michels and J. Loos, *Macromolecules*, 2004, **37**, 2151.
46 R. H. Lee and L. Y. Lee, *Colloid Polym. Sci.*, 2011, **289**, 1215.